REGULAR PAPER • OPEN ACCESS

Hierarchical super-hydrophobic coating with productive etching process and self-assembled Ag mask

To cite this article: Kazunari Tada *et al* 2025 *Jpn. J. Appl. Phys.* **64** 035001

View the article online for updates and enhancements.

You may also like

REGULAR PAPER

Hierarchical super-hydrophobic coating with productive etching process and self-assembled Ag mask

Kazunari Tada[1*], Tatsuya Naito[2*], and Yuji Honda[3*]

[1]Konica Minolta, Inc., Hachioji-shi, Tokyo, 192-8505, Japan
[2]Honda Motor Co., Ltd. Haga-gun, Tochigi, 321-3393, Japan
[3]You Patenter Co., Ltd. Funabashi-shi, Chiba, 273-0005, Japan

[*]E-mail: kazunari.tada@konicaminolta.com; tatsuya_naito@jp.honda; y-honda@you-patenter.com

Optical coating to maintain clear views in harsh environments is a vital technology to meet the increasing demand for vision assistance cameras or fully automated vehicles. In this study, the hierarchical nanostructured super-hydrophobic coating was fabricated without an expensive lithography process. First, the self-assembled Ag nano-mask was deposited on top of the SiO_2 layer instead of a lithography-patterned nano-mask. Next, isotropic etching to carve the SiO_2 layer and anisotropic etching to reshape the Ag nano-mask were alternatively applied to create a well-controlled hierarchical nanostructure of SiO_2 in one process. The size and pitch of the nanostructure were optimized by the deposition condition of Ag and the etching condition of Ag to gradually re-shape the Ag mask during the etching process. These techniques have achieved a productive etching process to form a rigid hierarchical nanostructure on a lens surface without a lithography technique. © 2025 The Author(s). Published on behalf of The Japan Society of Applied Physics by IOP Publishing Ltd

1. Introduction

Recently vision assistance cameras have gained increasing demands for drivers to recognize the surrounding road conditions that are normally out of view. They are also beneficial for partially autonomous vehicles to recognize the surrounding environment to ensure a safe drive. They have the advantages of being small, low cost, and high resolution compared to other sensors. However, one of the biggest challenges for these cameras is that they are required to maintain clear views even in rough road conditions such as rain, snow, or muddy roads. Normally, anti-reflection (AR) coating and conventional hydrophobic coating have contact angles of around 60° and 110°. Normal AR coating and conventional hydrophobic coating are deposited with the design of lens/SiO_2(30 nm)/OA600(30 nm)/SiO_2(30 nm)/TiO_2(113 nm)/SiO_2(88 nm), and lens/SiO_2(30 nm)/OA600(30 nm)/SiO_2(30 nm)/TiO_2(113 nm)/SiO_2(68 nm)/OA600(2 nm)/UD120(25 nm)/OR-510(5 nm) respectively. Here, OA 600 is a mixture of Ta_2O_5 and TiO_2 purchased from CANON OPTRON. For conventional hydrophobic coating, fluoride material (UD120, DAIKIN) and Non-fluoride material (OR-510, CANON OPTRON) are deposited on top of the surface in this order. However, these coatings are not hydrophobic enough for water droplets to roll off the surface to maintain a clear view of the camera. To approach this challenge, superhydrophobic coating with a contact angle of over 150° has been widely investigated as one of the promising solutions since it repels most obstacles to block a view away from a lens surface. For example, the mechanism of the superhydrophobic property of lotus leaves has been reported to consist of a hierarchical rough surface of micro and nanostructures with convex cells and epicuticular wax crystals on top of the structure.[1] Besides lotus leaves, there are many examples in nature that exhibit excellent superhydrophobicity with their unique microstructures on the surface. And numerous research has been reported to artificially mimic the microstructures on a substrate with various methods and materials.[2–6] For instance, the study of sol-gel wet coating is widely investigated to easily form a nanostructure.[7–10] While these techniques have the advantage of exploiting a cost-effective process, there is still room for improvement in terms of the durability against scrub tests because of its weak adhesion between the nanostructures and the substrate. Other techniques to fabricate nanostructures have been reported to overcome this weakness.[11–21] Among them, the etching technique is one of the promising candidates to achieve a robust superhydrophobic coating. Since etching is the technique that can carve materials to form nanostructures, the nanostructures are tightly integrated into a substrate with no bonding parts to degrade. However, one of the biggest challenges of the etching technique is that it normally requires expensive lithography technology to fabricate optimized nanostructures in terms of both optical properties and superhydrophobicity. For optical uses, reflectance, absorption, and scattering light need to be controlled below 1% so that the transmittance of light can be increased by more than 98%. To achieve the requirement, first, the size and depth of the nanostructure need to be smaller than the aimed wavelength to avoid excessive haze from Rayleigh scattering. Second, the depth of the nanostructure needs to be $\lambda/4$ to satisfy the index matching condition to exhibit anti-reflection properties. The nanostructure also must be optimized in shape, size, pitch, and depth to achieve superhydrophobicity at the same time. To meet these conditions simultaneously, it normally requires an expensive lithography process, which is not ideal for the cost effective mass production process. Previous studies[22–26] reported self-assembled block co-polymer masks can be a promising technique to eliminate the lithography process and lower the production cost. However, the controllability of nanostructure using block copolymer is 10 nm to 50 nm which is not the range that can achieve optical property and superhydrophobicity at the same time. To overcome this challenge, this study utilizes a self-assembled Ag mask to optimize the nanostructure in a range from 50 nm to 500 nm by changing the deposition temperature and thickness. It also employed isotropic and anisotropic alternate etching processes to change the size of the Ag mask
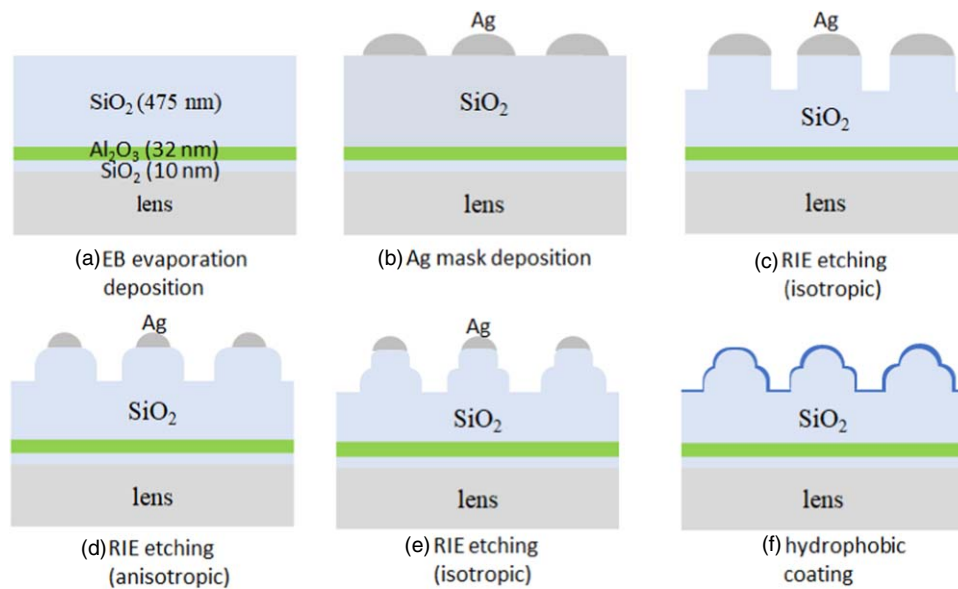
Fig. 1. Process flow of hierarchical nanostructure consisting of the first step and the second step.

in the middle of the etching to form hierarchical structures in a depth direction without a secondary mask deposition process. This technique can provide an opportunity that modify the structure in shape, size, and pitch in-depth direction while satisfying the ideal optical property and superhydrophobicity simultaneously without a lithography process.

2. Experimental method

2.1. Process flow

Figure 1 shows the fabrication process for the hierarchical nanostructure in this paper. First, the underlayers of SiO_2, Al_2O_3, and SiO_2 are prepared in this order on a lens surface using electron beam deposition with the thickness of 10 nm, 32 nm, and 475 nm respectively. Subsequently, a self-assembled Ag nano-mask was deposited on the underlayer with the thickness of 22 nm and the temperature of 160 °C. Next, reactive isotropic CHF_3 dry etching was employed to engrave the first rigid and durable nanostructure into the SiO_2 layer. A chemical reaction between the SiO_2 layer and CHF_3 accelerates the etching rate shown in Eq. (1)

$$3SiO_2 + 4CHF_3 \rightarrow 3SiF_4 + 4CO + 2H_2O \qquad (1)$$
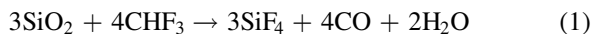
Here, the Ag mask was just exposed to physical plasma ion etching without chemical reaction. Then, anisotropic CHF_3 dry etching process was introduced to modify the shape of the Ag mask. After reshaping the Ag mask, the second isotropic CHF_3 dry etching process was applied so that a hierarchical nanostructure consisting of two different sizes was formed on top of the SiO_2 layer. These procedures were repeated several times to form the ideal secondary nanostructure with a round shape. After the etching process, the Ag mask was removed by aqueous potassium iodide solution and the lens was cleaned by ultrasonic with purified water. Next, the structure was cleaned by ion beam of Ar in a vacuum chamber and immediately the hydrophobic materials were coated on top of the fabricated hierarchical nanostructure to enhance the hydrophobicity. Lastly, to solidify the

hydrophobic material on the lens surface, 12 hours of the aging process was conducted at the environment of 120 °C.

2.2. Process

2.2.1. Preparation of multi-layer.
Since car cameras are normally desired to have a wide range of FOV (field of view), the lens preferably has a high refractive index of over 1.8. To avoid high reflectance of light, it is necessary for multi-layer to be designed to match the large gap of index between 1.8 of a lens and 1.0 of air. The layers are designed using Macleod under the assumption that the index of the first nanostructure is 1.3 and the depth is 100 nm. Similarly, the second nanostructure was assumed that the index is 1.1 and the depth is 100 nm. With this assumption, the design of the multi-layer was decided to be lens/SiO_2(10 nm)/Al_2O_3(32 nm)/SiO_2(475 nm)/Air. With this model, the simulation of reflectance was found to be well-matched to measured reflectance. The third layer of SiO_2 needs to be deposited thick enough to meet both anti-reflection property and superhydrophobic properties which requires the depth of nanostructures deeper than 200 nm. Ion beam assist and a high temperature of the substrate over 160 °C are necessary for the SiO_2 layer to have an excellent isotropic etching property which makes it easier to control the shape of the nanostructure during the etching process.

2.2.2. Self-assembled Ag mask.
Since the nanostructure needs to be fabricated on the curved surface of a lens, the lithography technique designed for the planar substrate cannot be applied. Also, it is more economical if nano masks can be fabricated in a controlled manner without a lithography process. Several self-assembled masks have been previously studied as a simplified nano-fabrication method[8–10]. In this paper, a self-assembled Ag layer is applied as a mask fabrication process to easily form a nanopattern on the curved surface of a lens without any lithography process. Since Ag is a well-known material that easily tries to form a nano agglomeration, it was possible to control the nanostructure if the deposition conditions were carefully optimized. The Ag nano-mask was deposited using a conventional thermal evaporation machine (BES,
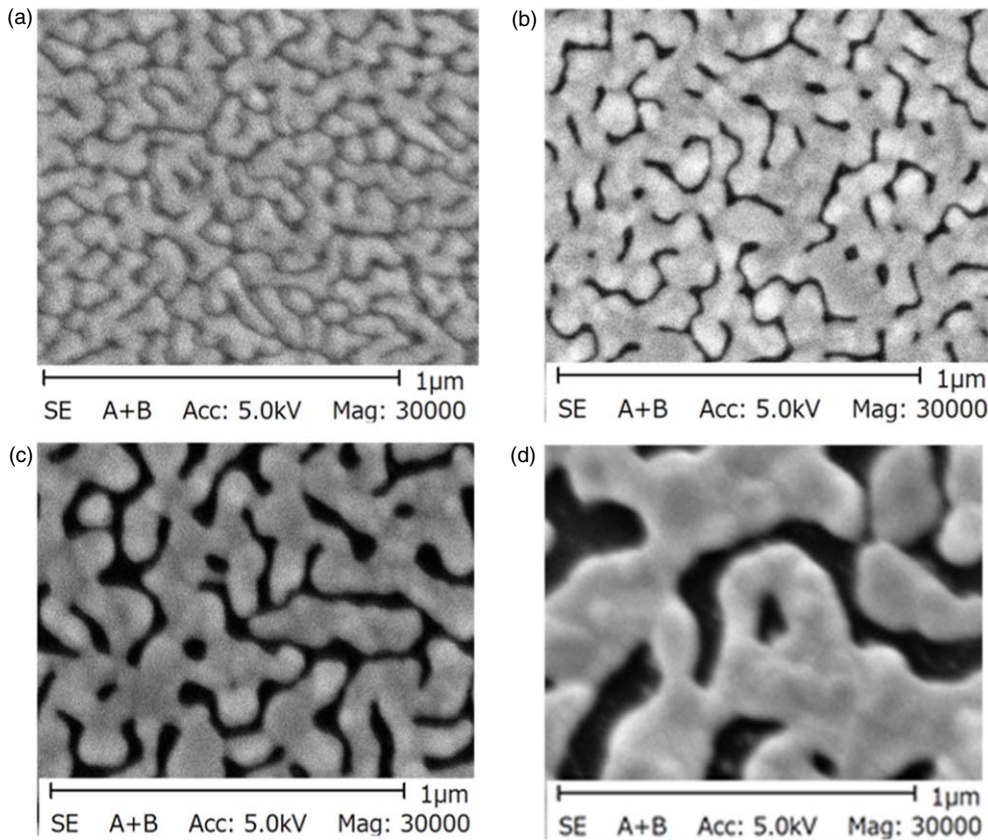
Fig. 2. SEM images of self-assembled Ag nanostructure mask at different depositing conditions. (a) Ag 14 nm at 144 °C, (b) Ag 20 nm at 150 °C, (c) Ag 20 nm at 172 °C, (d) Ag 39 nm at 300 °C.

SHINCRON). It was found that the deposition rate, the temperature of a substrate, and the thickness of the Ag layer were vital to control the gap and pitch of the Ag nano-mask (Fig. 2). The size of the Ag nanostructure was controlled smaller than the visible wavelength to decrease light scattering to enhance the transmittance. The gap and size were also adjusted so that the lens showed superhydrophobic property after the whole fabrication process was completed. It was determined that the optimal thickness of the Ag nano-mask was 22 nm, the temperature of the substrate was 160 °C, and the deposition rate of Ag was 1 Å s^{-1} to achieve both less light scattering and superhydrophobic properties.

2.2.3. Etching. Normally multiple mask fabrications and multiple etching processes are necessary to form a hierarchical etched structure. However, it leads to an extra fabrication cost and decreases the yield as the number of process step increases. To avoid the extra process, alternate isotropic and anisotropic etching processes were invented while maintaining good control of the etched structure. The important factor for isotropic etching was found that the temperature of the substrate needs to be below 35 °C to reduce the damage to

the Ag mask and increase the etching rate for the SiO$_2$ layer, which leads to a well-controlled vertical etching of SiO$_2$ due to the high selectivity of the Ag mask. On the other hand, the vital factor for anisotropic etching is to increase the temperature of the substrate to modify the Ag mask in shape and size in preparation for the secondary isotropic etching. Since the Ag mask gets damaged and changes in shape and size under high temperature of the plasma, plasma power, and the duration were optimized so that the Ag mask was re-shaped to an appropriate secondary mask. At the same time, anisotropic etching plays a very important role that rounding the sharp edges of the etched SiO$_2$ nanostructure to dramatically decrease the roll-off angle of water droplets. The round shape can be obtained during the anisotropic etching process because the high-temperature plasma etches the Ag mask, however, it etches the exposed SiO$_2$ layer at a very slow rate. Based on these key factors, isotropic and anisotropic etching conditions were determined in Table I. Pulse RF plasma was employed to enhance the temperature contrast between isotropic and anisotropic etching in addition to the change of input power. When the pulse is on, the plasma

Table I. Alternate etching condition of the isotropic and anisotropic process.

	Etching condition							
	isotropic	anisotropic	isotropic	anisotropic	isotropic	anisotropic	isotropic	anisotropic
CHF$_3$ (sccm)	70	70	70	70	70	70	70	70
APC (Pa)	10	10	10	10	10	10	10	10
Power (W)	300	800	300	800	300	800	300	800
Pulse	ON	OFF	ON	OFF	ON	OFF	ON	OFF
Time (s)	2400	700	800	300	300	300	200	200
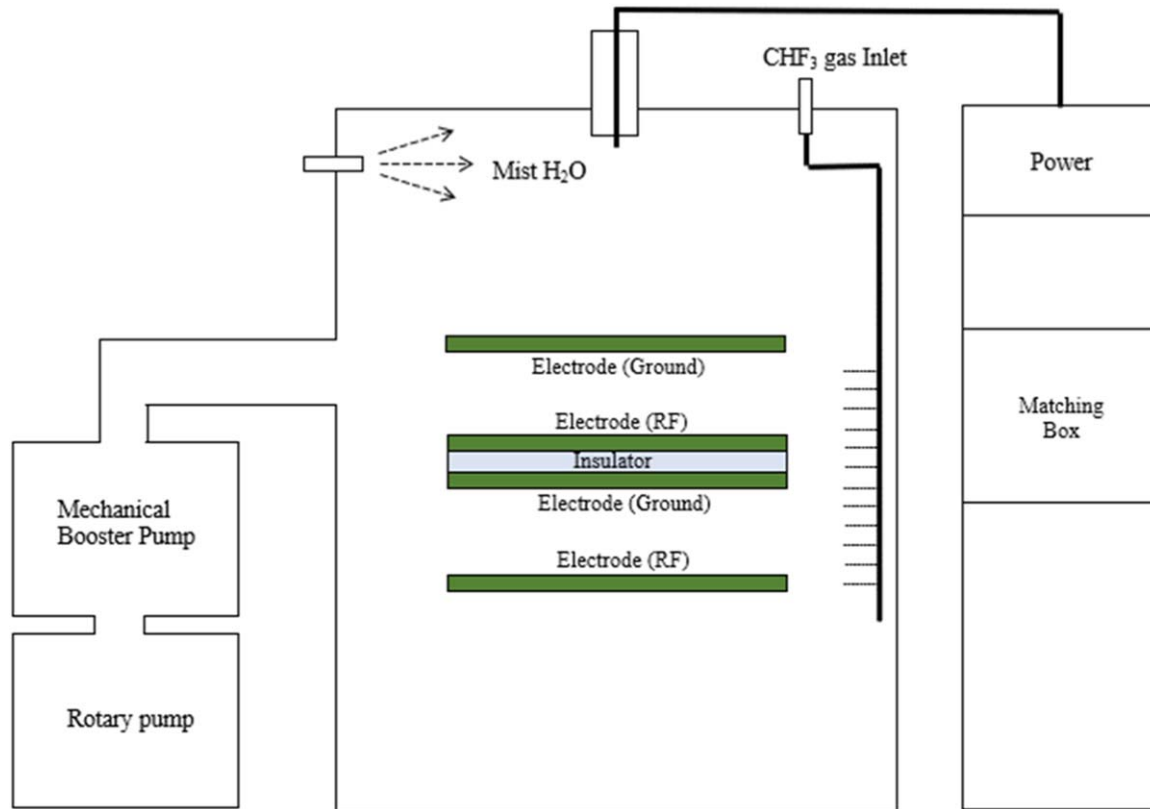
Fig. 3. Etching machine for mass production with large multiple electrodes.

temperature decreases effectively because the power source switches on and off at the frequency of 1 kHz with the duty ratio of 50%. The etching rate of SiO_2 can remain intact due to the very short duration of off time during which reactive agent gas is still active.

2.2.4. Shape of nanostructure. The nanostructure from the initial isotropic etching has a network structure with a depth of 100 nm. The network shape is effective to improve the durability of the SiO_2 structure. The nanostructure from the second isotropic etching has a shallow and round pea pod shape which is found to be beneficial in three ways. First, the round shape encourages water droplets to roll off the surface smoothly even if the depth of the structure is shallow. Second, the shallow and round pea pod shape is helpful to prevent the structure from breaking when the surface is scrubbed. Third, the round shape of the structure is useful to prevent the deposited hydrophobic material from peeling off the structure. If the nanostructure has a sharp edge, the hydrophobic material on top of the edge is difficult to adhere tightly and causes a peeling problem especially when it is rubbed. The peeling of hydrophobic material at the edge leads to a pinning effect that prevents the water droplet from rolling off the surface even if it maintains a high contact angle of over 150°.

2.2.5. Cleaning and hydrophobic coating. After the etching process, the residual Ag mask was removed by spraying KI solution on the sample. Then, the sample was cleaned with pure water using an ultrasonic cleaning machine. Followingly, Al_2O_3 and OA600 layers were deposited on top of the structure with the thicknesses of 20 nm and 2 nm respectively using an EB evaporation machine (BIS, SHINCRON). The Al_2O_3 layer was deposited to harden the surface of SiO_2, and the OA600 layer was deposited as an

undercoat for fluoride hydrophobic material to enhance the hydrophobicity. Lastly, 20 nm of UD120, and 5 nm of OR-510 were deposited in this order using thermal evaporation deposition (Gener-1300, OPTRUN). After the deposition, the sample was baked in a high-temperature oven of 120 °C for 12 hours to fixate the coating.

2.2.6. Etching machine. A new etching machine was invented for the mass production. A normal etching machine is designed for the semiconductor industry which has a process area of 16 inches at its largest. However, the mass production of optical lenses larger than semiconductor chips needs a much larger process chamber to accommodate as many lenses as possible. The new etching machine was modified based on the commercial CVD machine (You Cube, You-patenter). Figure 3 shows the new etching machine with a process chamber of 1 m^3. There were three important factors to achieve a big etching machine. First, multiple plasma electrodes are necessary to maximize the process area. It is equipped with two sets of plasma electrodes with an area of 65 cm^2. The lower Cu plates were connected to an RF power source of 1KHz, and the upper Cu electrodes were connected to ground wires from the chamber wall. The two sets of electrodes had stacked each other across the insulator. Second, the plasma electrodes need to be cooled down below 35 °C during the process. Circulating cooling water was introduced inside each copper electrode by chiller systems to lower the temperature of the electrodes. Cooling the sample temperature below 35 °C is extremely crucial for chemical reactive etching of SiO_2 to have a decent etching rate. When the temperature is increased, the etching rate of SiO_2 significantly decreases. Conversely, the Ag mask starts getting damaged from the high-temperature plasma resulting

Table II. Conditions of the environmental test.

Item	Test condition
120 °C	1,000 h in ST-120 (ESPEC)
−40 °C	1,000 h in SH-661 (ESPEC)
70 °C95%	1,000 h in SH-661 (ESPEC)
Abrasion	2,000 reciprocating scratches with a load of 250 g cm^{-2} with Tribogear (SHINTO Scientific)

in a low mask selectivity. The cooling water was designed to flow inside the Cu plasma electrodes to keep the temperature low during the etching process. Third, a novel neutralizer of toxic HF gas needed to be invented. Most of the reactive etching process leaves toxic gas of HF as a byproduct, which is very difficult to purge using a normal vacuum process alone. Normally, an etching machine for semiconductors has a load lock chamber to prevent toxic gas from directly releasing into the room, however, the large etching machine needs a different technology to neutralize the gas to avoid increasing costs for the large load lock chamber. To deal with the problems, mist H_2O was introduced into the chamber to capture HF gas after the etching process was completed. The fine mist of H_2O immediately vaporized in the vacuum chamber while capturing HF gas. These gases are easily purged out of the chamber using a vacuum pump which leads to the normal detoxification devices.

2.2.7. Characterization. The haze value was evaluated using a haze meter (NDH5000SP, NIPPON DENSHOKU INDUSTRIES) and the reflectance of the superhydrophobic coating was measured with a reflectance measuring machine (USPM-RU III, Olympus). The contact angle was measured using a contact angle meter (G-1, ERMA) based on the procedure

of JTS R3257 with the 10 μl of a water droplet. Environmental tests were also conducted for the coating with the conditions shown in Table II. For the abrasion test, a flat glass substrate was used instead of a lens substrate to evaluate because it is difficult to evenly scratch the curved surface of the lens. A flat abrasion head with wet clean paper was evenly contacted to the flat glass sample and scratched 2,000 times with a load of 250 g/cm^2.

3. Results and discussion

3.1. Evaluation of lens

3.1.1. Initial property. A hierarchical nanostructure was fabricated on top of the curved lens surface (Fig. 4). As can be seen, the nanostructure is optically clear due to the optimized size and depth of the structure below the wavelength of visible light. Also, there is no undesired diffraction pattern of light due to the random shape of the nanostructure, which is hard to achieve with a lithography technique. The haze value from light scattering was measured to be 0.5, which is clear enough for optical uses. The reflectance of the coating was well controlled below 1% after the etching process which showed a good match to the simulation design (Fig. 5). Then, the contact angle of the water droplet was compared between normal AR coating, conventional hydrophobic coating, and superhydrophobic coating shown in Fig. 6. While the conventional hydrophobic coating has a contact angle of 115 degrees, the superhydrophobic coating shows above 150 degrees. Water droplet on superhydrophobic coating easily rolls off the surface due to the lotus effect of micro and nanostructures and fluoride coating on top of it. The surface roughness of each coating was also compared between the coatings to relate the influence of the lotus effect on hydrophobicity (Fig. 7).
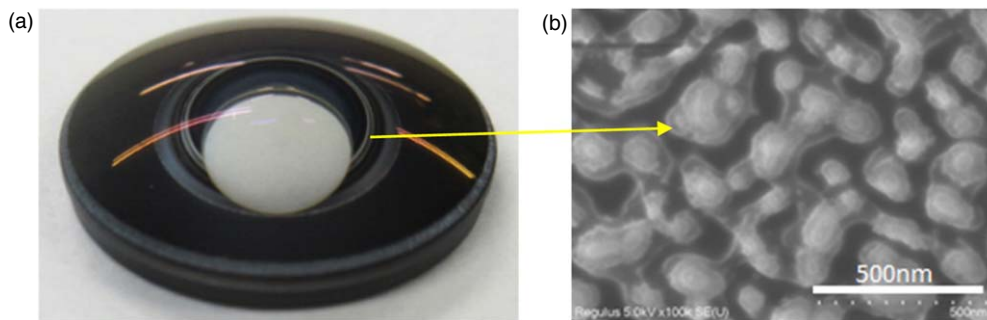
Fig. 4. (a) Photograph of the lens after all processes, (b) the SEM image of the surface of the lens.
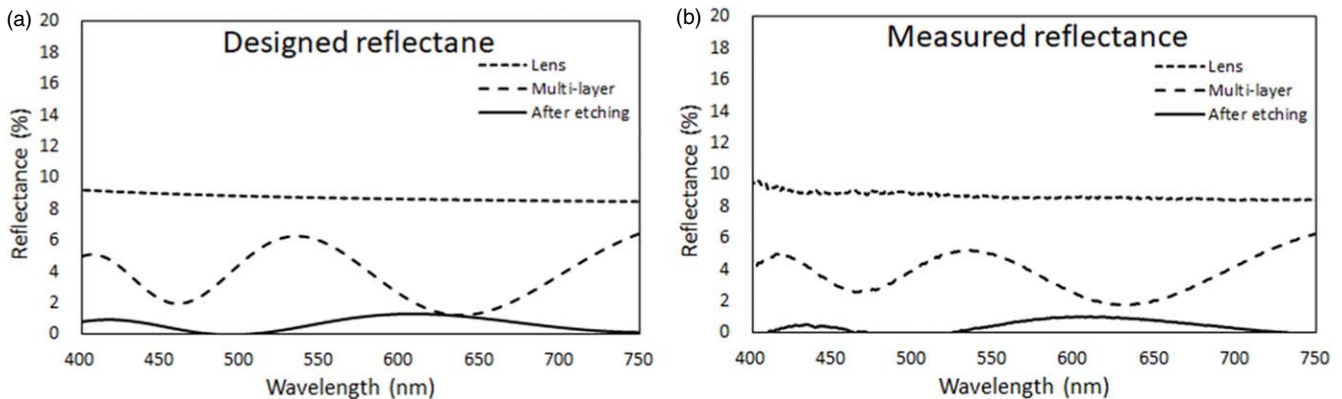
Fig. 5. Reflectance of a lens without coating (dotted line), with a multi-layer coating (broken line), and after the etching process (solid line) between (a) simulation and (b) measurement.
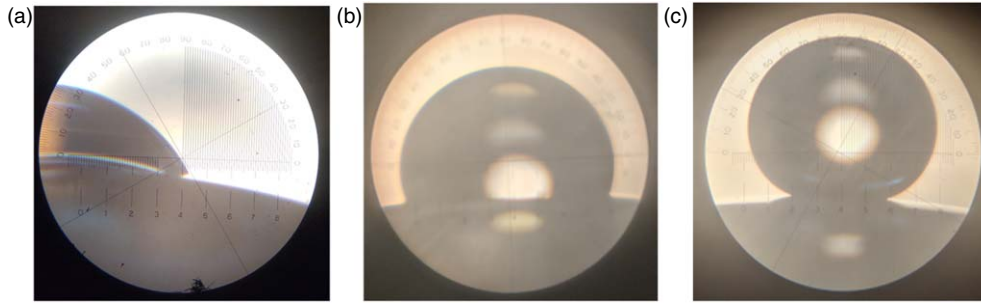
Fig. 6. Comparison of contact angle of the water droplet on a lens surface between (a) 58° for normal AR coating, (b) 115° for conventional hydrophobic coating, and (c) 151° for superhydrophobic coating.
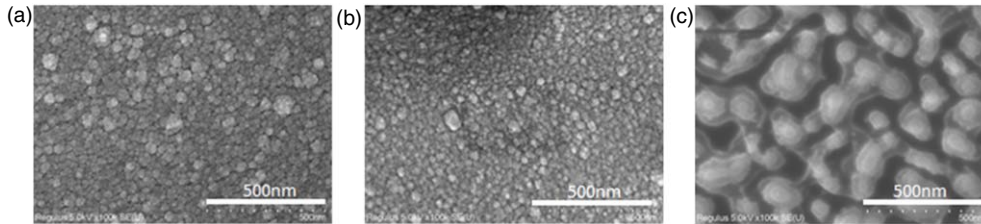
Fig. 7. Comparison of surface roughness between (a) normal AR coating, (b) conventional hydrophobic coating, and (c) superhydrophobic coating.
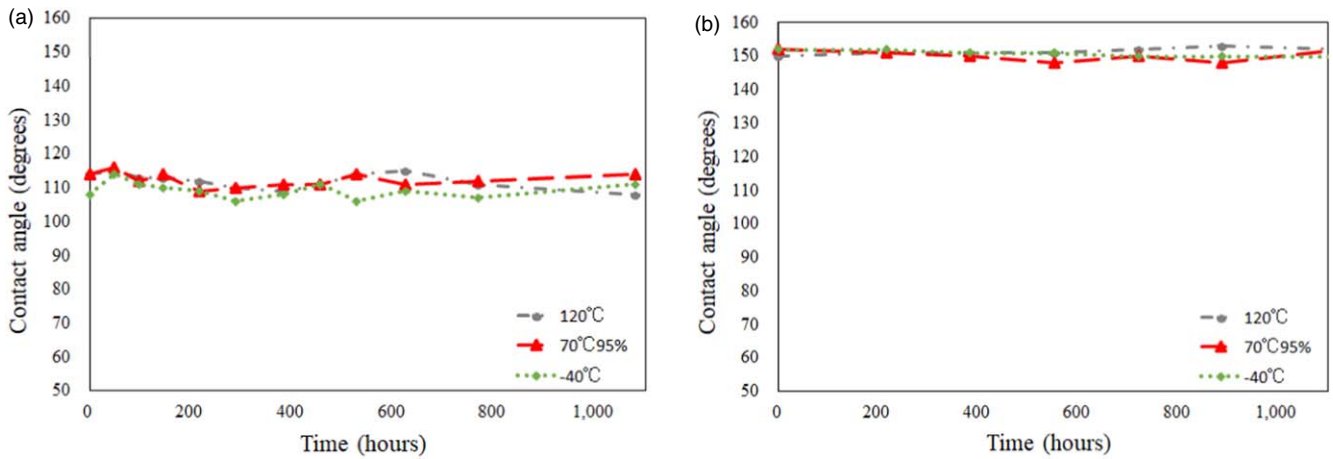
Fig. 8. Changes of contact angle over time against environmental tests. (a) conventional hydrophobic coating, (b) superhydrophobic coating.
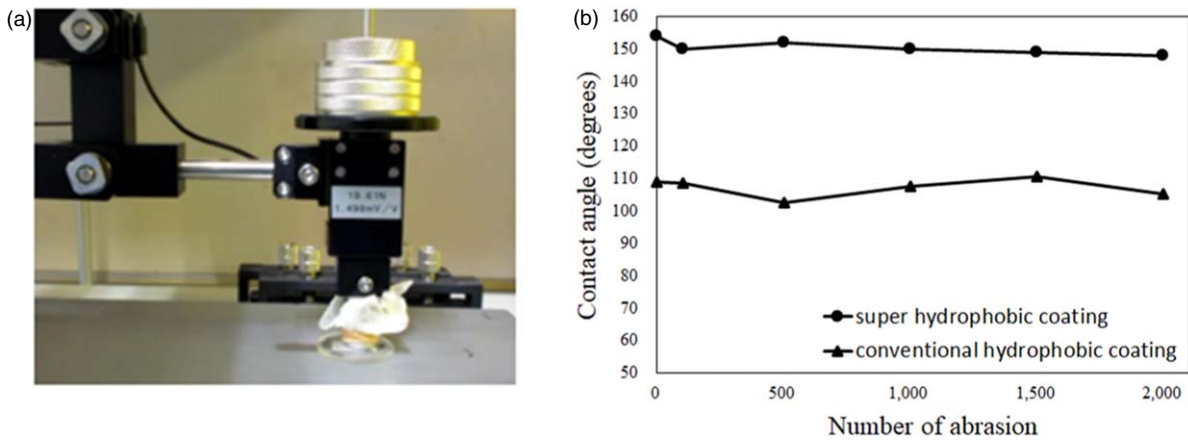
Fig. 9. Evaluation of abrasion test (a) equipment set up with the load of 250 g/cm^2, (b) result of contact angle over a number of abrasions between superhydrophobic coating and conventional hydrophobic coating.
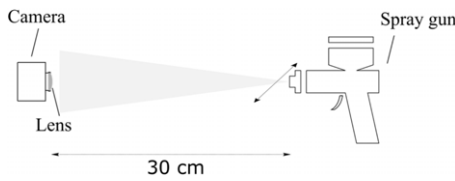
Fig. 10. Schematics of spraying dirt onto the lens surface.
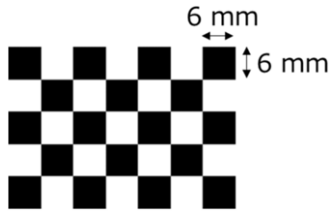
Fig. 11. Test chart to evaluate the image quality.
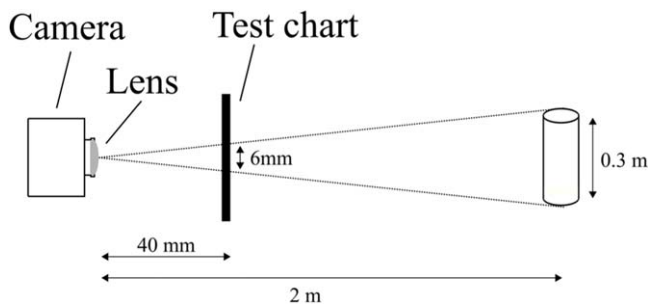
Fig. 12. Schematics of camera and test chart.

3.1.2. Environmental tests. Since car cameras are exposed to different road conditions, various environmental tests need to be cleared for the practical use of a commercial camera. Figure 8 shows the result of accelerated environmental tests which are required for typical car-mounted cameras. As can be seen, the coating maintains an initial performance of above 145 degrees of contact angle over 1,000 hours against

the tests. These results indicate that the performance can endure the practical use as a car-mounted camera. Also, an abrasion test was conducted to ensure the robust features of the hierarchical nanostructure as shown in Fig. 9. The contact angle of superhydrophobic coating was over 145 degrees after 2,000-reciprocating scratches with the load of 250 g/cm^2 due to the optimized rigid SiO_2 structure.

3.2. Evaluation of image quality

3.2.1. Setting and procedure. Car cameras mounted outside are exposed to harsh conditions such as splashes of water, ice melt salt, and mud from wheels depending on the road condition. The dirt from splashes causes image degradation of the camera when they are attached to the lens surface.[27–29] Superhydrophobic lenses in this paper were evaluated with dirts by comparing a normal AR coating lens and a conventional hydrophobic lens. These lenses were mounted on a commercially available USB camera (See3CM CU55 e-consystems) with a field of view of (H:200, V:160) which is comparable to a normal car-mounted camera. Next, three types of solutions were prepared in the form of water, water of ice melt salt (20 wt% of NaCl), and muddy water (20 wt% of Arizona test dust A4 coarse). Followingly, each liquid was sprayed uniformly to lens surfaces using an airbrush (Wider4 12J2:ANEST IWATA) from a distance of 30 cm to simulate an actual water splash from wheels (Fig. 10). For ice melt salt and muddy water, the sprayed solution on the lenses were naturally dried and the set of procedure was repeated four times to confirm the accumulation effect of the dirts. After spraying each dirt, the image quality was evaluated by taking pictures of a black and white test chart (Fig. 11). The distance between the lens and the chart was set to be 40 mm, in which one dot in the chart is equivalent to the size of 30 cm at the distance of 2 m from the lens (Fig. 12).

3.2.2. Comparison of image quality. Figure 13(a) shows the comparison of image quality after the water splash test. Normal AR coating shows the image degradation with an area of 7 dots at the center of the chart which indicates that the objects of 2.1 m at the distance of 2 m away from the lens

Fig. 13. Evaluation of image quality with the dirt of (a) water splash, (b) snow melting agent water, and (c) muddy water.

are barely visible due to water droplets. Conventional hydrophobic coating shows the image degradation with the area of 3 dots at the center of the chart which suggests that the objects of 0.9 m at the distance of 2 m from the lens are barely visible. On the other hand, the superhydrophobic coating in this paper doesn't show any degradation of image quality from a water splash to ensure a completely clear view for a car-mounted camera. Similarly, Figs. 13(b) and 13(c) show the comparison of image quality after the splash test of ice melt, salt water, and muddy water respectively. In both cases, superhydrophobic coating kept a completely clear view without any ice melt salt or muddy water attached to the lens surface. Considering these results from the splash test, only the superhydrophobic lens in this paper consistently shows a clear image throughout the tests which is a promising solution to the practical car-mounted camera.

4. Conclusion

Durable superhydrophobic anti-reflection coating with hierarchical nanostructure was successfully demonstrated. First, the fabrication process of durable hierarchical nanostructure imitating lotus leaves was introduced along with the self-assembled Ag nano-mask fabrication process which is suitable for the curved surface of a lens and for the mass production process. Then, the performance of superhydrophobicity and durability were evaluated through environmental tests and abrasion tests. Lastly, the image quality was proven to be intact when splashes of water, ice melt salt, and mud were applied to the surface.

1) M. Yamamoto, N. Nishikawa, H. Mayama, Y. Nonomura, S. Yokojima, S. Nakamura, and K. Uchida, "Theoretical explanation of the lotus effect: superhydrophobic property changes by removal of nanostructures from the surface of a lotus leaf," Langmuir **31**, 7355 (2015).
2) H. J. Ensikat, P. Ditsche-Kuru, C. Neinhuis, and W. Barthlott, "Superhydrophobicity in perfection: the outstanding properties of the lotus leaf," Beilstein J. Nanotechnol. **2**, 152 (2011).
3) C. Xu, R. Feng, F. Song, X-L. Wang, and Y-Z. Wang, "Desert beetle-inspired superhydrophilic/superhydrophobic patterned cellulose film with efficient water collection and antibacterial performance," ACS Sustainable Chem. Eng. **6**, 14679 (2018).
4) S. Barthwal, S. Uniyal, and S. Barthwal, "Nature-inspired superhydrophobic coating materials: drawing inspiration from nature for enhanced functionality," Micromachines **15**, 391 (2024).
5) X. Liu, Y. Liang, F. Zhou, and W. Liu, "Extreme wettability and tunable adhesion: biomimicking beyond nature?," Soft Matter. **8**, 2070 (2012).
6) J. Huang, X. Wang, and Z. L. Wang, "Controlled replication of butterfly wings for achieving tunable photonic properties," Nano Lett. **6**, 2325 (2006).
7) S. L. Dhere, S. S. Latthe, C. Kappenstein, G. M. Pajonk, V. Ganesan, A. V. Rao, P. B. Waghe, and S. C. Gupta, "Transparent water repellent silica films by sol–gel process," Appl. Surf. Sci. **256**, 3624 (2010).
8) D. K. Jean-Denis Brassard, Sarkar, and J. Perron, "Fluorine based superhydrophobic coatings," Appl. Sci. **2**, 453 (2012).
9) R. Taurino, E. Fabbri, M. Messori, F. Pilati, D. Pospiech, and A. Synytska, "Facile preparation of superhydrophobic coatings by sol-gel processes," J. Colloid Interface Sci. **325**, 149 (2008).
10) R. V. Lakshmi, T. Bharathidasan, and B. J. Basu, "Superhydrophobic sol–gel nanocomposite coatings with enhanced hardness," Appl. Surf. Sci. **257**, 10421 (2011).
11) B. H. Luo, P. W. Shum, Z. F. Zhou, and K. Y. Li, "Preparation of hydrophobic surface on steel by patterning using laser ablation process," Surf. Coat. Technol. **204**, 1180 (2018).
12) M. Bai, H. Kazi, X. Zhang, J. Liu, and T. Hussain, "Robust hydrophobic surfaces from suspension HVOF thermal sprayed rare-earth oxide ceramics coatings," Sci. Rep. **8**, 6973 (2018).
13) S. Khan, G. Azimi, B. Yildiz, and K. K. Varanasi, "Role of surface oxygen-to-metal ratio on the wettability of rare-Earth oxides," Appl. Phys. Lett. **106**, 061601 (2015).
14) I-K. Oh et al., "Hydrophobicity of rare Earth oxides grown by atomic layer deposition," Chem. Mater. **27**, 148 (2014).
15) Y. Song, R. P. Nair, M. Zou, and Y. Wang, "Superhydrophobic surfaces produced by applying a self-assembled monolayer to silicon micro/nano-textured surfaces," Nano Res. **2**, 143 (2009).
16) H. Hu, V. V. Swaminathan, M. R. Z. Farahani, G. Mensing, J. Yeom, M. A. Shannon, and L. Zhu, "Hierarchically structured re-entrant microstructures for superhydrophobic surfaces with extremely low hysteresis," J. Micromech. Microeng. **24**, 095023 (2014).
17) J. W. Bo Zhang and X. Zhang, "Effects of the hierarchical structure of rough solid surfaces on the wetting of microdroplets," Langmuir **29**, 6652 (2013).
18) D. Wang et al., "Design of robust superhydrophobic surfaces," Nature **582**, 55 (2020).
19) F. Su and K. Yao, "Facile fabrication of superhydrophobic surface with excellent mechanical abrasion and corrosion resistance on copper substrate by a novel method," ACS Appl. Mater. Interfaces **6**, 8762 (2014).
20) N. Wang, D. Xiong, Y. Deng, Y. Shi, and K. Wang, "Mechanically robust superhydrophobic steel surface with anti-icing, UV-durability, and corrosion resistance properties," ACS Appl. Mater. Interfaces **7**, 6260 (2015).
21) H. Jin, X. Tian, O. Ikkala, and R. H. A. Ras, "Preservation of super-hydrophobic and superoleophobic properties upon wear damage," ACS Appl. Mater. Interfaces **5**, 485 (2013).
22) M. A. Rad, K. Ibrahim, and K. Mohamed, "Formation of SiO_2 surface textures via CHF_3/Ar plasma etching process of poly methyl methacrylate self-formed masks," Vacuum **101**, 67 (2014).
23) S. Krishnamoorthy, C. Hinderling, and H. Heinzelmann, "Nanoscale patterning with block copolymers," Mater. Today **9**, 40 (2006).
24) W. I. Park, Y. J. Kim, J. W. Jeong, K. Kim, J-K. Yoo, Y. H. Hur, J. M. Kim, E. L. Thomas, A. Alexander-Katz, and Y. S. Jung, "Host-guest self-assembly in block copolymer blends," Sci. Rep. **3**, 3190 (2013).
25) J. Zheng et al., "Top-down fabrication of high-uniformity nanodiamonds by self-assembled block copolymer masks," Sci. Rep. **9**, 6914 (2019).
26) P. Ruchhoeft et al., "Patterning curved surfaces: template generation by ion beam proximity lithography and relief transfer by step and flash imprint lithography," J. Vac. Sci. Technol. B **17**, 2965 (1999).
27) A. J. Meuler et al., "Relationships between water wettability and Ice adhesion," Acs Appl. Mater. Inter. **2**, 3100 (2010).
28) P. Eberle, M. K. Tiwari, T. Maitra, and D. Poulikakos, "Rational nanostructuring of surfaces for extraordinary icephobicity," Nanoscale **6**, 4874 (2014).
29) J. Lv, Y. Song, L. Jiang, and J. Wang, "Bio-inspired strategies for anti-icing," ACS Nano **8**, 3152 (2014).